Isotopic disequilibrium during rapid crustal anatexis: implications for petrogenetic studies of magmatic processes

ELSEVIER

Chemical Geology 162 (2000) 169–191

CHEMICAL GEOLOGY
INCLUDING
ISOTOPE GEOSCIENCE

www.elsevier.com/locate/chemgeo

Isotopic disequilibrium during rapid crustal anatexis: implications for petrogenetic studies of magmatic processes

Gareth R. Davies *, Simone Tommasini [1]

Faculteit der Aardwetenschappen, Vrije Universiteit, De Boelelaan 1085, 1081 HV Amsterdam, Netherlands

Received 19 March 1998; received in revised form 10 December 1998; accepted 16 March 1999

Abstract

The geochemical consequences of crustal anatexis are investigated over a range of mineral dissolution rates; 10^{-10} cm/s (Mono Lake, CA), $\sim 10^{-16}$ cm/s (Seram, Indonesia) and $< 10^{-16}$ cm/s (regional migmatite terranes). Isotopic disequilibrium is established in all cases but surprisingly elemental partition coefficients appear close to equilibrium. This observation indicates that the melting and segregation rates are rapid enough to prevent full isotopic equilibration but that diffusion operates over a sub-100-μm length scale. A disequilibrium melting model is proposed in which diffusion maintains chemical equilibrium between the outer portions of minerals and melt but does not achieve full isotopic equilibrium between the entire protolith and melt. Preservation of isotopic disequilibrium in many metamorphic rocks has widespread implications. Dating metamorphic rocks using mineral–whole rock or mineral–mineral pairs may yield erroneous ages, as observed in the metasediments of Seram where ages range from −15 to 201 Ma, despite anatexis at ∼6 Ma. Consequently, some age estimates in the literature may be incorrect. Mono Lake is an example of how rapid melting will produce a sequence of chemically and isotopically distinct melts that are in isotopic disequilibrium with their crustal source. Hence, quantitative prediction of assimilation–fractional crystallisation (AFC) and anatectic processes requires full knowledge of the melting relations of the protolith. The chemical and isotopic disequilibrium associated with anatexis suggests that Nd model ages of granites and their protoliths will be incorrect when garnet and/or minor phases control a significant amount of the REE budget.

Keywords: Isotopic disequilibrium; Rapid crustal anatexis; Petrogenesis; Magma

1. Introduction

The composition of an anatectic melt is controlled by the physical conditions of melting and the time scale of the entire thermal event proceeding and associated with melting. At the simplest level, phase relations will result in major element differences between the efficient extraction of small degree, but heterogeneous, melts and the slower extraction of larger degree, more homogeneous, melts. There are two parameters that will determine if anatectic melts and their residua reach trace element and isotopic equilibrium. The first is the prograde history of the protolith. For example rapid heating events in rela-

* Corresponding author.
[1] Present address: Dipartmento di Scienza del Suolo e Nutrizione della Pianta, Piazzale delle Cascine 16, 50144 Firenze, Italy.

0009-2541/00/$ - see front matter
PII: S0009-2541(99)00123-0

tively shallow parts of the crust do not allow time for full isotopic equilibration between the minerals of the protolith. In contrast, it could be argued that the higher ambient temperatures of deeper crustal levels would maintain isotopic equilibrium in the protolith prior to anatexis in the lower crust. The observation of numerous disequilibrium and reaction textures in metamorphic rocks seen at the Earth's surface today implies that chemical equilibrium may not be the general rule (Yardley, 1995). Although many of these textures are a consequence of retrograde reactions this is not always the case and hence the possibility of widespread isotopic disequilibrium in protoliths must be assessed. If isotopic equilibrium is not achieved in the protolith then the second parameter, the time scale of melt extraction, will also influence the nature and extent of chemical fractionation between protolith and melt.

In this work, we examine trace element and isotopic evidence to determine which chemical model is most applicable to crustal anatexis and also place constraints on how the time scale of melting and melt extraction affects chemical and isotopic equilibrium. A basic question to be addressed is the extent to which trace elements obey Henry's law: i.e., is partitioning between melt and residue controlled by equilibrium partition coefficients? (e.g., Hart and Allégre, 1980). If trace elements obey Henry's law then melt extraction can be modelled as batch melting, when melt and residue remain in chemical equilibrium throughout the extraction process (e.g., Gast, 1968) or fractional melting where batch melts are immediately extracted from the residue and subsequently accumulated (e.g., Hanson, 1977).

Alternatively, melting may be a disequilibrium process during which chemical equilibrium is not fully maintained between residual phases and the melt. There are two possible scenarios that may operate during disequilibrium melting. The first, in which diffusion is sufficiently slow to prevent inter- and intra-mineral elemental and isotopic equilibration in the residue but chemical equilibrium is preserved between the melt and the portion of phases contributing to the melt. This situation is best envisaged by considering relatively slow mineral dissolution of, for example, a zoned plagioclase. The plagioclase rim alone contributes to the melt and achieves chemical equilibrium so that partition coefficients operate, at least on a sub-grain size scale. The melt will have the $^{87}Sr/^{86}Sr$ ratio of the plagioclase rim (i.e., not in isotopic equilibrium with the whole grain) and Sr contents will be low because of the high plagioclase–melt Sr partition coefficient. When mineral dissolution rates greatly exceed the rate of element diffusion within minerals, melt–mineral partitioning does not obey Henry's law and equilibrium partition coefficients do not operate: i.e., the effective partition coefficients ($K_{d\ \mathrm{Effective}}$) are equal to 1. If we again consider a zoned plagioclase, the Sr content and $^{87}Sr/^{86}Sr$ will simply be the weighted averages of the section of the grain that has been melted. Most previous workers have assumed the first scenario in which equilibrium partition coefficients operate during crustal melting, i.e., $K_{d\ \mathrm{Effective}} = K_{d\ \mathrm{Equilibrium}}$; $K_{d\ EF} = K_{d\ EQ}$ (Allégre and Minster, 1978; Prinzhofer and Allégre, 1985; Barbey et al., 1989; Bédard, 1989). Others have, however, argued that equilibrium partition coefficients do not operate (e.g., Bea, 1996). The aim of this work will be to use well-constrained and rapid melting events to assess if $K_{d\ EF} \neq K_{d\ EQ}$ and if conditions exist in nature where $K_{d\ EF} = 1$.

Over the last 2 decades, our understanding of crustal melting has evolved radically, often through the application of models from material sciences. In the 1980s, the use of fluid dynamic concepts led to the conclusion that two phase flow (compaction) was inefficient at the relatively high viscosities of crustal melts (10^4 to 10^{11} Pa s). Therefore, over the time scales of most major thermal events (< 10 Ma) there would be limited melt–source separation even at large degrees of melting ($> 10\%$; McKenzie, 1985; Wickham, 1987a; Miller et al., 1988). Consequently, there was a general consensus that large bodies of relatively homogeneous granitic magma could only form as a consequence of:

(i) large degrees of melting (30–50%) and/or;

(ii) hydrous melts with low viscosity.

These conditions would allow convective motion and compaction to operate more efficiently (Wickham, 1987a; Miller et al., 1988). Authors, therefore, favoured extended periods of melt–protolith contact and hence a batch equilibrium melting model. The enigma, however, was the ample evidence that relatively small degree melt fractions can segregate into batholith-sized bodies (e.g., Miller et al., 1988) and

that there is no evidence that *all* granitic magmas have the high water contents to give viscosities of the order of 10^2 Pa s (see review by Baker (1996)). Although melt extraction due to fracturing was initially dismissed as a local phenomenon (e.g., Miller et al., 1988), more recent numerical analysis implies that melt extraction and migration are most efficient under conditions of fracture propagation (Emerman and Marret, 1990; Clemens and Mawer, 1992; Petford et al., 1993; Sawyer, 1994). This conclusion raises the possibility that coupled rapid rates of melting and extraction may not result in isotopic and chemical equilibration between melts and crustal protoliths.

It is now well-established that the diffusion coefficients of Pb, Sm, Nd and Sr (i.e., elements used in isotopic studies) are low in many minerals at, or close to, anatectic temperatures ($< 10^{-16}$ cm^2/s, see review by Brady (1995)). Previous workers have formulated expressions that describe the effective partition coefficient of a mineral as a function of crystal growth/dissolution rate, diffusion coefficient and equilibrium partition coefficient (e.g., see Henderson and Williams, 1979; Hart and Allégre, 1980). When effective diffusion coefficients are $< 10^{-16}$ cm^2/s one can predict that full chemical equilibrium will not be maintained during a melting event if mineral dissolution rates exceed 10^{-18} cm/s. It is, however, difficult to predict the actual elemental diffusion coefficients and diffusive distances within residual minerals. The uncertainty partly comes from the fact that experimental diffusion coefficients are determined on gem quality phases assuming an infinite reservoir. In contrast, minerals in metamorphic rocks have numerous lattice defects (e.g., Watson, 1996) and are involved in multi-component mineral reactions. It is, therefore, to be expected that the effective elemental diffusion length scales in metamorphic minerals are below the observed grain size. This is the reason that many workers assume that chemical disequilibrium is not important during anatexis. Consequently, a goal of this work is to use examples of anatexis to constrain the actual diffusive length scale of elements within residual minerals and so establish if the typical time scale of crustal anatexis and melt extraction will cause the entire process to be in chemical and isotopic equilibrium. Due to the slow diffusion of Sr in feldspars, which are major rock-forming minerals (Giletti, 1991a; Cherniak and Watson, 1992, 1994; Giletti and Casserly, 1994; Cherniak, 1996), this study will concentrate on the Sr isotope system.

The above discussion is not simply an academic exercise. Crustal anatexis is one of the major processes that control the chemical differentiation of the continental crust, producing an upper crust that is enriched in the heat producing elements U, Th and K (e.g., Fyfe, 1973; Rudnick, 1992). These elements control the thermal budget and the rheology of the upper crust, which in turn may influence near surface tectonics and landform development. It is, therefore, important to establish the details of crustal anatexis to allow realistic quantification of chemical and thermal models of the crust.

2. Examples of rapid anatexis

In order to fully assess if chemical and isotopic equilibrium are preserved during partial melting, the source–melt relationship must be unambiguous. Ideally, the source should be old, so that minerals have very distinct isotopic ratios and the melting should be young, so that there is no need for large corrections in determining initial isotopic ratios. Here, we consider the chemical consequences of two anatectic events with unambiguous source–melt relations that respectively produce 10 m^3 and > 1 km^3 of melt. The rapid nature of both examples provide opportunities to examine if $K_{\mathrm{d\ Equilibrium}} \neq K_{\mathrm{d\ Effective}} = 1$ in nature. Later, we will compare these examples with large scale migmatite terranes in a general overview to assess how widespread melt–source trace element and isotopic disequilibrium is in the crust.

2.1. Mono Lake, Sierra Nevada, CA

Melting of the Rattlesnack Gulch granite, part of the Cretaceous Sierra Nevada batholith northwest of Mono Lake, CA (93 ± 3 Ma; Chesterman, 1968) was caused by trachyandesite. The melt–source relationships can be unambiguously identified in the field as melt migration was limited. Moreover, the age of melting is relatively young (11.9 Ma; Kaczor et al., 1988; Tommasini and Davies, 1997). Unfortunately,

the relatively young granite protolith does not contain minerals with extreme Nd and Pb isotopic ratios. Details of the textural and geochemical relationships between granite melts and residual granite phases have been reported in three previous studies (Al-Rawi and Charmichael, 1967; Kaczor et al., 1988; Tommasini and Davies, 1997). The most pertinent points are the following.

(a) An approximately circular trachyandesite plug, roughly 50 m in diameter, intrudes the granite and is related to a single magmatic event.

(b) Melting of the granite at the contact is limited to a narrow zone 2–3 m wide and reaches a maximum of 10–20%. The unmelted granite has an hypidiomorphic medium- to coarse-grained texture and consists of quartz, andesine/oligoclase (core An_{40}, rim An_{15}, Table 1), microperthitic orthoclase/microcline (Or_{90}) and biotite (mol $Mg/(Mg + Fe) = 0.4$, Table 1), with accessory apatite, zircon, oxides and allanite.

(c) Blocks of granite, up to 4×4 m, occur within the plug and experienced up to 75% melting.

(d) Contacts between partially melted granite and the trachyandesite magma are sharp but locally quenched trachyandesite xenoliths (1 mm to 10 cm) are found in the glass and xenocrysts of quartz, plagioclase and alkali feldspar are ubiquitous in the trachyandesite within 1 m of the granite contacts.

(e) The partially melted granite has an hypocrystalline groundmass enclosing residual quartz, plagioclase sanidine/anorthoclase, fine-grained biotite breakdown products (rutile, orthopyroxene, oxides) and minor phases (e.g., zircon, apatite). Residual anorthoclase grains have a spongy texture. Where unaltered glass consists of light-brown and dark-brown phases that contain microlites of quartz and feldspar which probably nucleated during rapid cooling. The light-brown phase is prevalent in the granite with lower melting degrees (contact zone) and around quartz grains, whereas the dark-brown glass is prevalent in the granite with higher degrees of melting. The two glass phases are not a consequence of liquid immiscibility since in thin section they display gradational contacts.

Samples representative of both the melted granite and trachyandesite were collected in order to assess

Table 1
Major element analyses of the granite and partially melted granite from Mono Lake

	6708 Granite	6700 A1 HIGH glass brown	6700 A2 HIGH glass brown	6700 A1 HIGH glass white	6700 A2 HIGH glass white	6707 D1 LOW glass brown	6707 D1 LOW glass white	6707 E LOW glass white	6707 F LOW glass white
n	1	6	6	6	5	12	5	11	22
SiO_2	72.63	73.95 ± 0.29	73.80 ± 0.41	79.43 ± 0.48	79.42 ± 0.35	77.88 ± 0.41	77.80 ± 0.49	78.42 ± 0.58	78.50 ± 0.45
TiO_2	0.25	0.26 ± 0.02	0.28 ± 0.03	0.06 ± 0.04	0.08 ± 0.05	0.20 ± 0.05	0.19 ± 0.02	0.22 ± 0.04	0.23 ± 0.04
Al_2O_3	14.49	14.23 ± 0.18	14.37 ± 0.13	11.13 ± 0.38	11.43 ± 0.34	12.46 ± 0.14	12.39 ± 0.24	12.23 ± 0.36	11.80 ± 0.21
FeO	1.89	1.57 ± 0.05	1.58 ± 0.04	1.26 ± 0.16	0.98 ± 0.33	0.83 ± 0.08	0.74 ± 0.10	0.93 ± 0.17	0.96 ± 0.07
MnO	0.05	0.06 ± 0.02	0.05 ± 0.02	0.03 ± 0.01	0.03 ± 0.01	0.02 ± 0.02	0.03 ± 0.01	0.02 ± 0.01	0.03 ± 0.02
MgO	0.52	0.36 ± 0.02	0.37 ± 0.03	0.22 ± 0.01	0.18 ± 0.06	0.11 ± 0.01	0.09 ± 0.03	0.19 ± 0.18	0.06 ± 0.02
CaO	1.85	0.61 ± 0.05	0.63 ± 0.04	0.27 ± 0.03	0.28 ± 0.05	0.29 ± 0.02	0.27 ± 0.03	0.32 ± 0.03	0.40 ± 0.05
Na_2O	3.39	2.00 ± 0.10	1.87 ± 0.19	1.59 ± 0.08	1.60 ± 0.05	1.91 ± 0.19	1.46 ± 0.32	1.64 ± 0.13	1.72 ± 0.18
K_2O	7.79	6.77 ± 0.29	6.86 ± 0.51	5.91 ± 0.18	5.93 ± 0.18	6.21 ± 0.20	5.99 ± 0.29	5.95 ± 0.24	6.20 ± 0.18
P_2O_5	0.07	bdl	bdl	bdl	bdl	bdl	bdl	bdl	bdl
BaO	0.14	0.11 ± 0.01	0.12 ± 0.04	0.05 ± 0.02	0.05 ± 0.02	0.02 ± 0.01	0.02 ± 0.01	0.01 ± 0.02	0.02 ± 0.02
F	nd	0.06 ± 0.04	0.05 ± 0.04	0.03 ± 0.03	0.00 ± 0.00	0.03 ± 0.02	0.01 ± 0.02	0.03 ± 0.03	0.06 ± 0.04
Cl	nd	0.02 ± 0.01	0.03 ± 0.01	0.02 ± 0.01	0.01 ± 0.01	0.02 ± 0.01	0.01 ± 0.01	0.02 ± 0.01	0.03 ± 0.01
LOI	0.30								
Total[a]	100.37	94.56 ± 0.72	94.96 ± 0.55	94.50 ± 0.36	95.26 ± 0.37	94.51 ± 0.31	94.68 ± 0.66	94.66 ± 0.43	94.65 ± 0.40
ASI	1.02	1.21 ± 0.02	1.23 ± 0.03	1.17 ± 0.01	1.19 ± 0.02	1.20 ± 0.05	1.33 ± 0.12	1.25 ± 0.07	1.15 ± 0.04

n = Number of analyses averaged ± 1 SD (standard deviation); nd = not determined; bdl = below detection limit. ASI = aluminium saturation index (mol $Al_2O_3/(CaO + Na_2O + K_2O)$).

[a] Glass analyses normalised to 100% with totals before normalisation.

the extent of (dis)equilibrium attained by the different minerals during the melting event. Hand specimens were cut into slabs for polished thin section preparation allowing minerals and unaltered glass to be microdrilled and microprobed. An unmelted granite sample (6708) of similar lithology to that of the melting region was collected 1 km south of the plug.

An estimate of the time scale of melting is required to quantify the rates of the physical and chemical processes that operated during anatexis at Rattlesnake Gulch. This has been achieved using a simple one-dimensional explicit finite difference thermal model (Tommasini and Davies, 1997). The points relevant to the assessment of isotopic disequilibrium during granite melting are:

(i) granite blocks inside the plug melt almost instantaneously, ca. 3 months;

(ii) maximum temperature reached by the granite blocks are roughly 1000°C after ca. 1.5 years;

(iii) the temperature of the entire system remains above 500°C for 40 years;

(iv) the country rock granite at the contact of the plug does not reach the solidus, though the temperature at 1 m from the contact rises to >700°C within a few months.

The discrepancy between this last conclusion and field observations of 10–20% melting at the contact is easily explained due to the 1-m space steps in the model and the assumption of instantaneous injection (see the work of Tommasini and Davies (1997) for more discussions). Granite phase relations suggest that the peak temperature ~ 1000°C is sufficient to cause the large extent of melting experienced by the granite blocks, though insufficient for total melting (e.g., Bohlen et al., 1995). The presence of residual feldspar, quartz and orthopyroxene is, therefore, consistent with the thermal model.

2.1.1. Major element data

Representative major element compositions of anatectic glasses are reported in Table 1 along with the source granite. In general the glasses are enriched in SiO_2 and depleted in K_2O, CaO, Na_2O and ferromagnesian elements with respect to their source granite (Fig. 1). The glasses can be broadly divided into two types that reflect liquids formed by low ($\sim 10\%$, 6707) and high ($\sim 70\%$, 6700) degrees of melting of the granite (henceforth for clarity referred to as LOW and HIGH, respectively). The former represents samples from the contact between the trachyandesite plug and the country granite, whereas the latter are samples from the granite block inside the plug. There is significant major element heterogeneity in glass compositions within a single thin section and most notably within 0.5 mm of residual phases. These latter chemical variations were interpreted as diffusion-controlled dissolution across a boundary layer at the solid–liquid interface (Zhang et al., 1989; Tommasini and Davies, 1997). Consequently, glass compositions reported in Table 1 were sampled >0.5 mm away from residual phases. The glass within each hand-specimen records marked variation in colour. The end member populations are manifested as light-brown and dark-brown glass. As a whole the LOW glass is enriched in K–feldspar and quartz components and notably depleted in ferromagnesian elements (Fig. 1) because it is representative of melts formed by biotite breakdown according to the reaction:

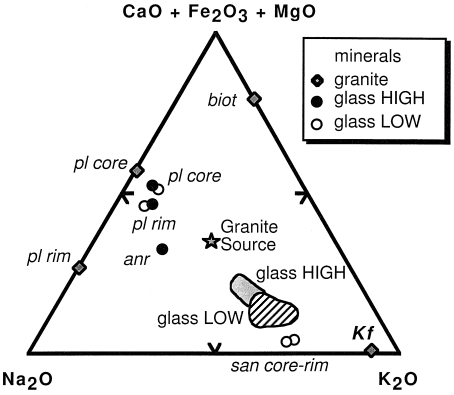

Fig. 1. Na_2O–K_2O–($CaO + Fe_2O_3 + MgO$) triangular diagram (mol%) for the granite, glasses and minerals. pl = plagioclase; san = sanidine; anr = anorthoclase; biot = biotite.

$$\text{biotite} + \text{quartz} + \text{feldspar} = \text{orthopyroxene} \pm \text{oxides} + \text{liquid}. \quad (1)$$

This conclusion is consistent with the higher values of the alumina saturation index (ASI = mol $Al_2O_3/(Na_2O + CaO + K_2O)$) of the glasses compared to the source granite (Table 1).

Within a thin section there are significant chemical differences between the dark and light glasses (Table 1) with the latter having notably greater SiO_2. Mass balance calculations demonstrate that the light glass is not simply a consequence of a greater quartz contribution to the melt. This lighter coloured glass appears to represent sampling of an almost pure end member of reaction (1). The HIGH glass is predominantly dark brown. The rare associated regions of light brown glass have similar compositions to the LOW glasses (Table 1). The dark brown HIGH glass contains 5 wt.% lower SiO_2 and significantly greater Al_2O_3, K_2O, TiO_2, FeO, MgO, CaO and Na_2O (Table 1). Although this composition is more comparable to the source granite composition, these data indicate that, compared to the LOW glasses, the HIGH glasses contain a greater contribution of plagioclase and potassium feldspar plus significant contribution from the biotite breakdown products (orthopyroxene and oxides, Fig. 1).

2.1.2. Sr–Nd–Pb isotope data

Sr–Nd–Pb isotope data for granite, glass, minerals and trachyandesite are reported in Tables 2 and 3. To establish the extent of isotopic homogeneity within the glass phases, Sr–Nd–Pb isotope analyses have been carried out on sub-samples from two rocks (HIGH 6700 and LOW 6707, Table 2) and a further six Rb–Sr isotope analyses of ~ 1 mg glass samples from ~ 1 cm^3 sub-samples of 6700 and 6707 (Table 2). The different glass samples were separated on the basis of colour by hand-picking

Table 2
Sr, Nd and Pb isotope data of the granite and the partially melted granite from the Rattlesnake Gulch

Sample	6708			Glass 6700					
	Granite source			HIGH-A1	HIGH-A2	HIGH-B1	HIGH-B2	Light	Dark
Details	wr	normal duplicate	duplicate in bomb	HP (0.5–1 mm)	< 2.4 (100–250 μm)	HP (0.5–1 mm)	< 2.4 (100–250 μm)		
Rb	230		235	288	299	273	278	307	285
Sr	293		296	86.07	66.36	98.74	77.53	45.24	84.12
Sm	2.953	2.835	2.935	3.903	3.597	4.202	3.904		
Nd	19.04	18.16	18.94	21.96	19.60	23.61	21.76		
U	9.29		9.11	8.21	8.68	6.18	6.26		
Pb	23.2		23.1	23.1	23.0	24.2	24.1		
$^{87}Rb/^{86}Sr$	2.274		2.296	9.676	13.03	8.001	10.39	19.54	9.804
$^{87}Sr/^{86}Sr_m$	0.70865	0.7086	0.70865	0.70963	0.71022	0.70916	0.70956	0.71145	0.70930
$^{87}Sr/^{86}Sr_{11.9\,Ma}$	0.70827	0.7083	0.70826	0.70799 ± 20	0.70802 ± 24	0.70781 ± 19	0.70781 ± 20	0.70813 ± 35	0.70765 ± 20
$^{147}Sm/^{144}Nd$	0.0936	0.0944	0.0937	0.1074	0.1109	0.1076	0.1085		
$^{143}Nd/^{144}Nd_m$	0.51251	0.51250	0.51250	0.51251	0.51251	0.51251	0.51250		
$^{143}Nd/^{144}Nd_{11.9\,Ma}$	0.51250	0.51249	0.51249	0.51250	0.51250	0.51250	0.51249		
$^{238}U/^{204}Pb$	26.1		25.6	23.0	24.5	16.6	15.9		
$^{206}Pb/^{204}Pb_m$	39.098		39.086	39.102	39.173	39.076	39.147		
$^{207}Pb/^{204}Pb_m$	15.687		15.682	15.683	15.707	15.678	15.699		
$^{206}Pb/^{204}Pb_m$	19.520		19.512	19.434	19.461	19.399	19.419		
$^{206}Pb/^{204}Pb_{11.9\,Ma}$	19.471		19.465	19.392	19.416	19.368	19.368		

Errors in measured (m) and initial ($i = 11.9$ Ma) represent $\pm 2\sigma$ run precision (only shown when greater than the reproducibility of standards) and $\pm 2\sigma$ propagated error. Uncertainties (2 SD) in U/Pb, Rb/Sr and Sm/Nd are < 2, < 1 and < 0.5%, respectively.
The external precision of standards: $^{67}Sr/^{86}Sr = 0.710278 \pm 18$ (2 SD, $n = 26$) for NIST SRM 987; $^{143}Nd/^{144}Nd = 0.511852 \pm 10$ (2 SD, $n = 25$) for La Jolla; $^{206}Pb/^{204}Pb = 36.512 \pm 13$, $^{207}Pb/^{204}Pb = 15.431 \pm 4$, $^{206}Pb/^{204}Pb = 16.894 \pm 3$ (2 SD, $n = 10$) for NIST SRM 981.
wr = whole rock; HP = hand-picked glass after sieving; < 2.4 = glass < 2.4 g/cm^3; $<$ and $>$ magn = relatively low and highly magnetic glass fractions.

from different density and magnetic fractions with the aim of sampling the chemically most extreme glasses from each sample. The combined Sr–Nd–Pb isotope data do not define mixing relationships between the granite and trachyandesite which establishes that, as implied by the observed field relations, the trachyandesite and granite melts have not mixed (Tommasini and Davies, 1997). Taken together, the Rb–Sr isotope glass data do not yield an isochron (MSWD > 100). This is reflected in extremely variable $^{87}Sr/^{86}Sr_{11.9\,Ma}$, with absolute differences up to 0.0017 (Fig. 2). The LOW glasses have Sr isotope compositions that are similar to, or significantly more radiogenic than, the source granite at 11.9 Ma. The light coloured glasses with the most radiogenic $^{87}Sr/^{86}Sr$ do not have the highest Rb/Sr ratio (Fig. 2). The HIGH glasses are all less radiogenic than the source granite at 11.9 Ma. Within the HIGH glasses there is a general positive correlation between $^{87}Sr/^{86}Sr_{11.9\,Ma}$ and Rb/Sr. Significant differences among glasses and the source granite are also observed for Pb isotopes (Table 2), with sample LOW-A having the most radiogenic composition. Accessory phases are known to play a fundamental role in controlling Pb isotope compositions during anatexis (e.g., Rapp and Watson, 1986; Hogan and Sinha, 1991; Zhang and Schärer, 1996). Although recognising that Pb isotope disequilibrium is preserved between source and melts we will not discuss these data further in this contribution. The marked differences in Sr and Pb isotopes contrast with constant initial Nd isotope ratios (Table 2). This homogeneity

Glass 6707							6705	6706
LOW-A	LOW-B1	LOW-B2	Light		Dark		Trachyandesite	
< 2.4 (100–250 μm)	< 2.4 < magn (100–250 μm)	< 2.4 > magn (100–250 μm)	A	B	C	D	wr	wr
427	352	325	308	303	387	413	39.0	53.9
30.01	27.11	29.16	29.37	31.37	33.43	27.93	1045	911.4
2.016							6.609	4.682
9.964							39.19	26.00
4.34	3.83	3.77					3.16	1.83
19.4	17.5	18.0					13.9	15.0
41.15	37.60	32.30	30.36	27.96	33.51	42.82	0.1080	0.1711
0.71571	0.71460	0.71433	0.71428	0.71407	0.71386	0.71561	0.70557	0.70570
0.70875 ± 70	0.70824 ± 64	0.70887 ± 55	0.70915 ± 52	0.70935 ± 79	0.70819 ± 58	0.70837 ± 73	0.70555	0.70567
0.1223							0.1020	0.1069
0.51251 ± 10							0.51255	0.51247
0.51250 ± 10							0.51254	0.51247
14.8	14.2	13.6					14.6	7.85
38.999	39.058	39.054					38.873	38.888
15.708	15.699	15.702					15.664	15.664
19.573	19.373	19.351					19.060	19.056
19.548	19.347	19.326					19.033	19.041

Table 3
Sr isotope data of minerals from the granite and partially melted granite

Sample	Mineral	Rb	Sr	$^{87}Rb/^{86}Sr$	$^{87}Sr/^{86}Sr_m$	$^{87}Sr/^{86}Sr_{11.9\,Ma}$
6708 Granite source	Kf rim	411	523.2	2.270	0.70851	0.70812
	Kf core	305	517.4	1.706	0.70777	0.70748
	pl rim	104	502.1	0.5974	0.70626	0.70615
	pl core	16.7	1112	0.0434	0.70558	0.70557
	Kf	309	481.1	1.856	0.70795	0.70764
	biot	960	31.66	88.78	0.82947	0.81447 ± 15
6700 HIGH-A glass	pl	69.9	467.0	0.4332	0.70777	0.70769
	anr	106	738.4	0.4152	0.70808	0.70801
6700 HIGH-B glass	anr	122	727.2	0.4842	0.70788	0.70780
6707 LOW-A glass	san	157	378.8	1.199	0.70841	0.70821
	pl	131	536.1	0.7048	0.70798	0.70786
	biot res	94.0	180.2	1.509	0.70863	0.70838

is expected given the relatively young age of the source granite, similar parent–daughter ratios of the major rock-forming phases in the granite and the long half-life of ^{147}Sm.

2.2. Seram, East Indonesia

The second example of anatexis is from the island of Seram, eastern Indonesia. Partial melting occurs in a simple tectonic setting due to obduction of oceanic lithosphere onto a monotonous series of pre-Triassic greenschist facies fine-grained (< 0.5 mm) graphitic metapelites and minor meta-arkoses (Linthout and Helmers, 1994). Rare lenses of metabasites are also found within the metasediments. Metapelites unaffected by the obduction-related metamorphism comprise quartz (20–30%) + oligoclase (20–30%) + biotite (40–50%) + musco-

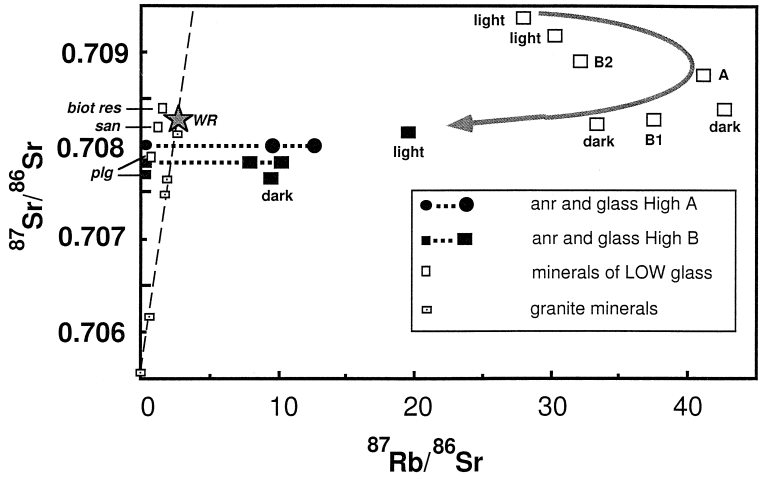

Fig. 2. $^{87}Sr/^{86}Sr$ vs. $^{87}Rb/^{86}Sr$ at 11.9 Ma for granite, glasses and residual minerals. The extreme Sr isotope disequilibrium between the different glass and mineral phases establishes that melting was a disequilibrium process. Sr isotope equilibration between anorthoclase and host glass, connected by dotted lines, is due to anorthoclase being a fine-grained reaction product. Glasses that represent relatively low and high degree melts define a trend (grey arrow) that indicates greater feldspar contribution as metling increases. anr = anorthoclase, plag = plagioclase, san = sanidine, biot res = residue after biotite breakdown.

vite (5–10%). Coarse-grained quartz veins up to 10 cm across are ubiquitous throughout the metasedimentary sequence and in all cases are formed prior to the last, emplacement-related deformation. Anatexis of the metasediments is limited to highly sheared mylonites that occur within a vertical distance of < 50 m from the base of the ophiolite. The mylonites contain migmatitic textures with biotite + plagioclase + quartz + sillimanite ± garnet melanosome and quartz + plagioclase + K–feldspar ± muscovite leucosome. Granites cut the ophiolite–sediment contact and are found in the overlying ophiolite. These S-type, cordierite-bearing granites have a restricted silica range ($SiO_2 = 74–76$ wt.%) and an ASI varying from 1.1 to 1.4 (Table 4). The granites are characterised by coarse-grained quartz aggregates similar to the quartz veins found in the metasediments. Granites also contain $\sim 5\%$ restitic xenoliths with gradational contacts (biotite + sillimanite + plagioclase + quartz ± cordierite ± garnet up to 10 cm in length). From current surface exposure we estimate that > 1 km^3 of granite was produced. Due to the extensive erosion it is possible that this is a significant under estimate.

Thermobarometric studies suggest that melting occurred at $\sim 0.4–0.5$ GPa and ~ 740°C through muscovite breakdown in the presence of sillimanite, plagioclase and quartz (Linthout and Helmers, 1994). Obduction occurred immediately prior to 6 Ma (Linthout et al., 1996). The most precise muscovite and biotite Ar–Ar ages obtained from the complex (5.90 ± 0.28 Ma and 5.51 ± 0.04 Ma, respectively) establish that cooling from ~ 400°C to 320°C occurred within a maximum of 700 ka and a minimum of 7 ka (Linthout et al., 1996). From palaeogeographic reconstructions, *P–T* estimates and thermal modelling, Linthout et al. (1996) concluded that the entire complex cooled from anatectic temperatures, 740°C, to the closure temperature of biotite in < 2.0 Ma. Thermal models indicate that rocks remained above 600°C for significantly less than 1 Ma (i.e., at temperatures where element diffusion is most significant). Field observations suggest that the migmatites underwent $\sim 5\%$ melting. If we assume that melting was confined to the peak of the thermal event then mineral dissolution rates must be greater than 4×10^{-17} cm/s and we consider the best estimate is 4×10^{-16} cm/s, assuming melting within 100 ka. In comparison to melt generation at Mono Lake, the thermal pulse on Seram is $> 10^3$ times longer but clearly maximum temperatures of the protolith were lower. Such melting rates are sufficiently slow that the diffusion rate of many elements (10^{-16} cm/s) may be greater and hence element partitioning during melting could be close to an equilibrium process.

2.2.1. Sr–Nd–Pb isotope data

Sr, Nd, and Pb isotope analyses are reported in Table 4 for the granites, metasediments, and metabasites. The granites and metasediments have Nd and

Table 4
Isotopic data from the granites, metasediments and metabasites of the island of Seram

Sample	Rock type	SiO_2 (wt.%)	ASI	$^{87}Rb/^{86}Sr$	$^{87}Sr/^{86}Sr_m$	$^{147}Sm/^{144}Nd$	$^{143}Nd/^{144}Nd$	$^{238}U/^{204}Pb$	$^{208}Pb/^{204}Pb$	$^{207}Pb/^{204}Pb$	$^{206}Pb/^{204}Pb$
BK6	granophyre	75.75	1.05	22.5	0.71901	0.2179	0.51211	18.6	38.916	15.646	18.744
BK19	granite	74.22	1.11	12.1	0.71727	0.1359	0.51220	4.30	38.990	15.674	18.742
BK18	granite	74.02	1.37	3.69	0.72700	0.1214	0.51208	5.32	38.954	15.666	18.740
BM42a	meta-arkose	80.82	1.51	2.81	0.72377	0.1218	0.51216	4.00	39.016	15.661	18.786
BM42c	metapelite	65.74	2.35	4.17	0.73223	0.1196	0.51208	4.18	39.047	15.669	18.776
BM42b	metapelite	64.90	2.24	4.17	0.73222	0.1264	0.51207	3.68	39.047	15.669	18.777
BK21[a]	metapelite	62.23	2.75	8.92	0.73582	0.1401	0.51204	9.29	39.079	15.676	18.801
BM42	metapelite	61.56	2.62	6.07	0.73243	0.1321	0.51209	4.88	38.986	15.652	18.748
BK28	metabasite	49.85		0.0964	0.70423	0.2086	0.51306	4.65	38.224	15.749	18.101
BK29	metabasite	49.65		0.164	0.70422	0.2099	0.51305	7.09	38.160	15.623	18.080

Isotopic analyses performed on a single sample dissolution. Errors in isotopic ratios as in Table 2. Major elements, and Rb and Sr concentrations were measured by XRF.

[a] Mylonitic metapelite < 50 m from the ophiolite–sediment contact.

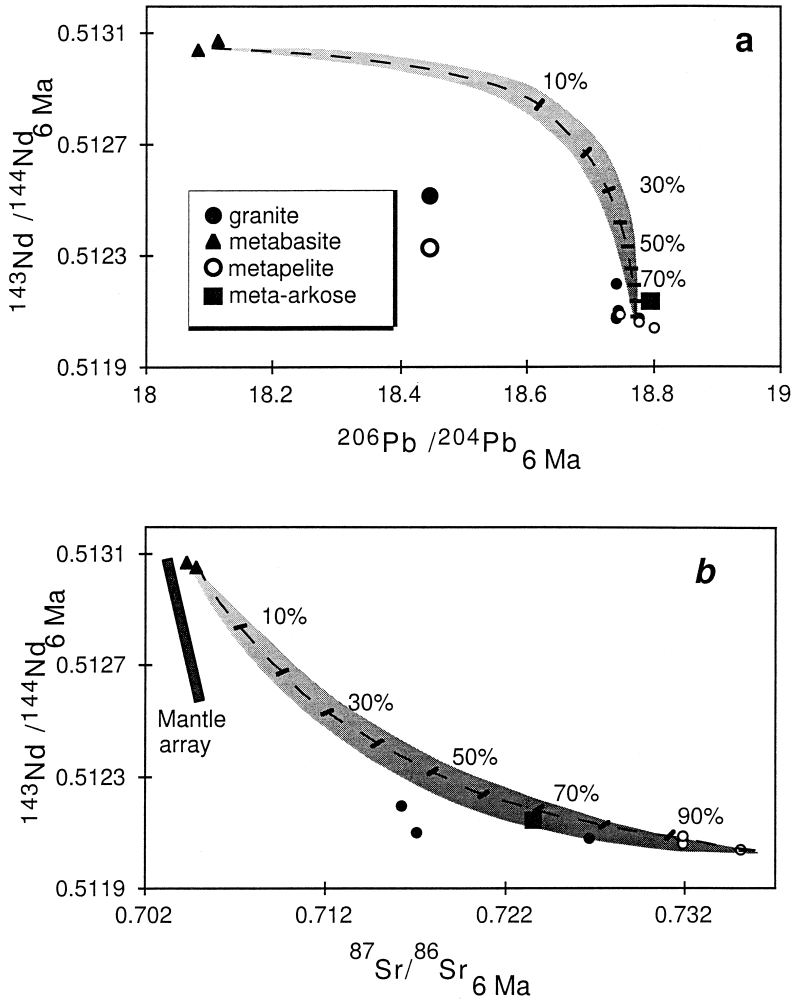

Fig. 3. $^{143}Nd/^{144}Nd_i$ vs. $^{87}Sr/^{86}Sr_i$ (a) and $^{143}Nd/^{144}Nd_i$ vs. $^{206}Pb/^{204}Pb_i$ (b) of the granites, metasediments and metabasites from the island of Seram. The mantle array is reported for comparison. Solid line: mixing line between average metasediment (metapelites and meta-arkose) and metabasite compositions (figures refer to weight percent (wt.%) of metasediment in the mixture). Grey area: all possible mixture between metasediments and metabasites. Note that the granites and metasediments have essentially identical Nd and Pb isotope compositions.

Pb isotope compositions that are identical but distinct from the lenses of metabasites found within the metasediments (Fig. 3a). In contrast, the granites have $^{87}Sr/^{86}Sr_{6\,Ma}$ that are up to 0.018 lower than the metasediments (Fig. 3b). The difference in Sr isotopes between the metasediments and granites cannot be explained by a contribution from the metabasites because: (i) at 750°C metabasites are not expected to melt, a conclusion confirmed by field studies; (ii) the granites and metasediments have similar Nd and Pb isotopes precluding a metabasite component (Fig. 3a); (iii) The Sr–Nd isotope relationships of the granites are not consistent with mixing between metasediments and metabasites (Fig. 3b).

Minerals from rock chips of both granites and metasediments were sampled using microdrilling techniques (Table 5). All metasediments, including

Table 5
Sr isotope data of minerals from the granite and partially melted granite

Sample	Rock type	Drilled material	Weight (mg)	Rb	Sr	$^{87}Rb/^{86}Sr$	$^{87}Sr/^{86}Sr_m$	Isochron type	Age (Ma)
BM42		matrix	2.09	345	187.5	5.343	0.73035	matrix–wr	201 ± 22
BM42a	meta-arkose	matrix	2.54	271	158.1	4.959	0.72475	matrix–wr	32.2 ± 1
BK21	metapelite	plagioclase	1.01	6.52	246.3	0.077	0.72763	plag–wr	65.2 ± 0.7
BK21 A	leucosome	muscovite	1.43	339	21.61	45.54	0.73344 ± 3		
	leucosome	quartz-rich	1.1	0.0165	0.797	0.0598[a,b]	0.71151 ± 3[a]	qtz-rich–musc	33.9 ± 0.6
	leucosome	plagioclase-rich	2.09	59.3	135.5	1.267	0.71370	plag-rich–musc	31.4 ± 0.3
	leucosome	plagioclase	0.21	1.88	318.7	0.0171[b]	0.72571 ± 3	plag–musc	12.0 ± 0.1
BK21 B	leucosome	plagioclase	0.73	3.80	476.3	0.0231	0.72787 ± 3		
	melanosme	matrix #1	1.66	338	50.57	19.37	0.72484 ± 2	matrix #1–plag	−11.0 ± 0.2
	melanosme	matrix #2	1.18	308	40.73	21.89	0.72329	matrix #2–plag	−14.7 ± 0.3
	melanosme	matrix #3	1.58	369	42.76	24.99	0.72314	matrix #3–plag	−13.3 ± 0.3
BK18	granite	feldspar	2.7	94.2	158.7	1.720	0.72479	feld–wr	79 ± 2
		feldspar	0.41	151	174.4	2.517	0.72628	feld–wr	44 ± 2
		feldspar	1.12	102	177.5	1.666	0.72405 ± 2	feld–wr	103 ± 2
		feldspar	1.19	95.2	166.5	1.657	0.72470	feld–wr	80 ± 2
		biotite	2.38	702	11.21	181.6	0.73911 ± 2	biot–wr	4.79 ± 0.05

Microdrilling was performed using a diamond-tipped drill on $2 \times 3.5 \times 0.5$ cm polished rock chips. Matrix samples taken from < 1 mm^3. BK 21, 21A, 21B are mylonitic metapelites with migmatite textures sampled within 50 m of the base of the ophiolite.
Analytical techniques as in Table 2.
[a]Corrected for a Sr blank of 50 pg.
[b]Corrected for a Rb blank of 50 pg.

migmatites, have large inter-mineral Sr isotope disequilibrium yielding two point ''isochrons'' ranging from 201 to −15 Ma (Table 5). Plagioclase–muscovite pairs from the leucosomes of BK 21A

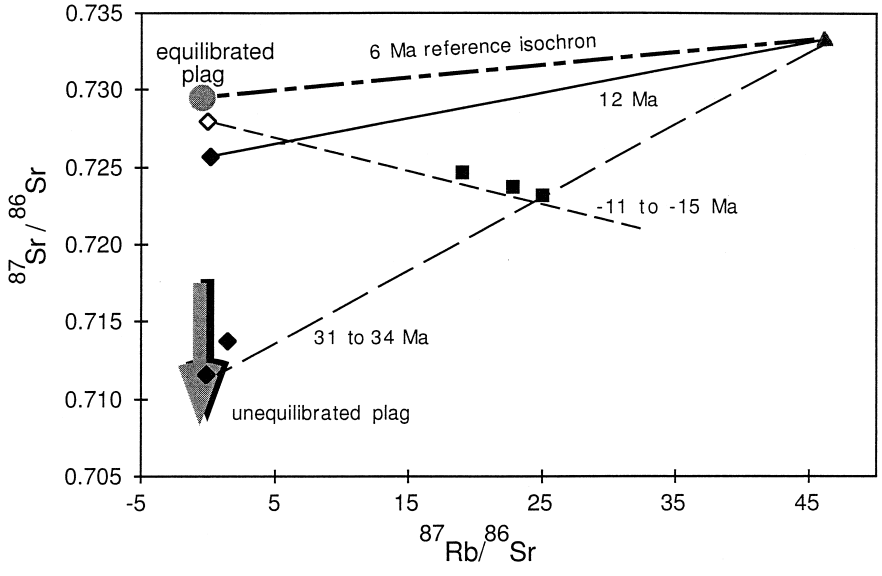

Fig. 4. $^{87}Sr/^{86}Sr$ vs. $^{87}Rb/^{86}Sr$ for the drilled portions of two migmatitic samples of the metapelite BK21 from the ophiolite–sediment contact. Closed symbols refer to BK21 A, open symbol to BK21 B. Circle: plagioclase (including quartz-rich and plag-rich samples) from the leucosome; triangle: muscovite from the leucosome; square: matrix from the melanosome. The 6-Ma reference isochron represents the expected age of the metamorphic and anatectic event (Linthout et al., 1996). The $^{87}Sr/^{86}Sr$ of predicted equilibrated (grey circle) and non-equilibrated (grey arrow) plagioclase are shown for reference.

yield Rb–Sr ''ages'' of 34 to 12 Ma (Fig. 4). In contrast, the plagioclase from the leucosome and the three matrix samples from the melanosome of BK 21B yield ''future ages'' from −11 and −15 Ma. A biotite–whole rock pair from the granite BK 18 yields an ''age'' of 4.8 Ma, whereas feldspar–whole rock pairs yield ''ages'' between 44 and 103 Ma (Fig. 4).

3. Discussion

3.1. Mono Lake

The hand-picked glass samples from Mono Lake are in marked Sr isotope disequilibrium, establishing that isotopic equilibrium was not attained on a centimeter scale even though temperatures reached ~1000°C. Most residual feldspars have not reached Sr isotope equilibrium with their host melts (Table 3). Glass–mineral pairs yield Rb–Sr ages that are up to 20% higher than the age of melting. Mineral–glass and mineral–mineral Sr isotope disequilibrium is most marked within the partially melted granite along the contact (LOW), probably due to the lower temperature reached by the country granite and lower degree of melting. These relationships are illustrated in Fig. 2, where the Sr isotope composition of minerals and glasses are reported at the time of melting. Mineral pairs define Rb–Sr ages (51–61 Ma) that tend to the Cretaceous emplacement age of the granite. The Sr isotope data from the glasses and residual minerals formed by granite melting provide compelling evidence for extreme isotopic heterogeneity even within handspecimens and demonstrate there was negligible melt homogenisation via diffusion and convection.

At Mono Lake melts were not separated from the protolith so that fractional melting models sensu stricto are not applicable. However, on the scale sampled in this study there is significant major and trace element variation in melt composition which is not consistent with a physical batch melting model. In terms of the current melting models the Mono Lake example could perhaps be argued to represent an heterogeneous chemical boundary layer that could ultimately yield melts that would mix during the extraction process. Current terminology is, however, difficult to apply in this case, but a process comparable to fractional melting appears to be required to explain the melt heterogeneity despite the lack of melt separation.

3.1.1. A disequilibrium melting model

The kinetics of solid-state diffusion provide an explanation for the marked Sr isotope disequilibrium preserved in the partially melted granite. Published Sr diffusion coefficients (e.g., Brady, 1995) establish that an almost instantaneous melting event will allow negligible resetting of $^{87}Sr/^{86}Sr$ among the major rock-forming minerals. Tommasini and Davies (1997) proposed a disequilibrium melting model in which partition coefficients operate to explain the observed Rb–Sr isotope systematics. During melting the Sr isotope composition of a melt depends upon the relative proportion of minerals contributing to the melt along with the solid–liquid distribution coefficient (K_d) of Sr for each mineral (i.e., the Sr budget contributed by each mineral). Fig. 5a is a schematic representation of how the Rb–Sr isotope systematics would change in successive liquids derived from a simple biotite–plagioclase source. The model is a good representation of the actual data (Fig. 2). Under this model the glasses with the most radiogenic $^{87}Sr/^{86}Sr$ represent a liquid originating early in the melting event dominated by biotite breakdown whereas glasses with greater Rb/Sr ratios and lower $^{87}Sr/^{86}Sr$ represent liquids with a relatively larger contribution from feldspar once most biotite has been consumed. The model of Tommasini and Davies (1997), although designed to explain isotopic disequilibrium, assumes that equilibrium K_d's operate between the melt and the residual mineralogy. Under such conditions early biotite breakdown will yield melts with low Rb/Sr (K_d Rb and Sr, respectively, high and low) and plagioclase derived melts would have relatively high Rb/Sr (K_d Rb and Sr, respectively low and high). If, as discussed earlier, the rate of melt formation is significantly greater than the rate of elemental diffusion, then chemical equilibration will not be maintained and partition coefficients cannot be used to predict the melt composition (i.e., $K_{d\,EF} \neq K_{d\,EQ}$).

An alternative melting model, shown in Fig. 5b, assumes that the linear mineral dissolution rates are

10^{-10} cm/s. The effective diffusional length scale in nature is an unknown which we are hoping to constrain from this study. For this model we have assumed it to be 10% of the observed grain size but this assumption has no bearing on the conclusions reached later. Again for simplicity only two phases are present: biotite and plagioclase. All initial melts are assumed to be in chemical equilibrium with the residual phase, even for elements with slow diffusion coefficients. With mineral dissolution rates several orders of magnitude greater than the effective rate of diffusion, subsequent melts will have trace element compositions essentially equal to those of the starting mineral. The trace element composition of a melt would simply be controlled by the elemental composition of the individual mineral phases contributing to the melt. Under conditions where the melting rate is less extreme, element fractionation will depend on the partition coefficient and the difference between the rate of melting and diffusion. Provided that the dissolution rate and effective diffusional grain size are known, effective partition coefficients ($K_{d\ EF}$) can be calculated by modification of the expressions used by Henderson and Williams (1979) and Hart and Allégre (1980). In the case considered in Fig. 5b, the diffusion of Sr in plagioclase is low (Cherniak and Watson, 1994; Cherniak, 1996) such that after the formation of initial melts from grain boundaries, Sr partitioning into the melt would be a disequilibrium process and that the effective partition coefficient ($K_{d\ EF}$) would be close to 1. Rb diffusion in feldspars (Giletti, 1991a) is significantly faster than Sr but is still insufficient to allow chemical equilibration with the inferred melting rates and hence $K_{d\ EF}$

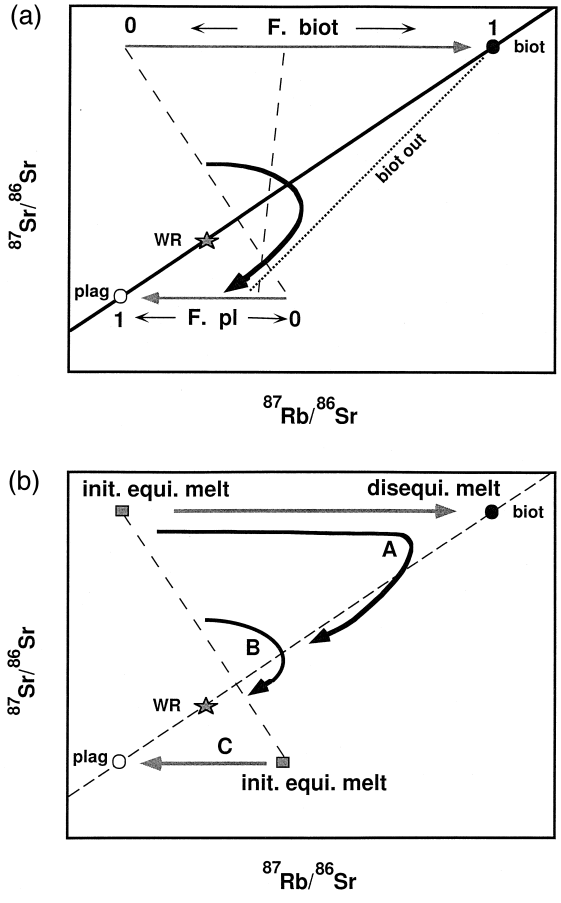

Fig. 5. (a) Schematic diagram illustrating the consequences of disequilibrium batch or fractional melting during anatexis in a simple two component system (biotite and plagioclase). Such a scenario is predicted when the rate of element diffusion is greater than the melting rate such that the chemical equilibrium is maintained between melt and residual phases, i.e., partition coefficients opperate. The minerals in the protolith of an arbitrary age define an isochronous relationship (solid black line). The grey arrows represent the evolution of melt compositions from biotite and plagioclase as the degree of melting increases (F from 0 to 1). Initial melts are biotite-rich. Dashed lines represent possible mixtures of melts from plasioclase and biotite. Thick curved arrow is a hypothetical evolution of successive liquid fractions when the melting rate of biotite is greater than of plagioclase. (b) Schematic diagram illustrating the consequences of disequilibrium melting during anatexis in a simple two component system (biotite and plagioclase) where partition coefficients do not operate. Symbols as in (a). Under this scenario the melting rate is much greater than chemical diffusion. Initial melts will be controlled by equilibrium element partitioning but subsequent melts will have Rb/Sr ratios close to the mineral phases and, therefore, lie on, or close to the granite isochron. The thick curved arrows represent hypothetical evolutions of successive liquid fractions derived under different plagioclase to biotite melting ratios. Curve A represents melts that are initially derived from biotite breakdown with plagioclase only contributing to the melt at a later stage. Once melting is established, new melts will lie close to the granite isochron. Curve B represents melts that are initially derived predominately from biotite breakdown but mixing with plagioclase derived melts with higher Sr contents means that melts will have less extreme Rb/Sr ratios than curve A. Predicting actual melt compositions, even in this simple two component system, requires a knowledge of the melting relations and the efficiency to which the different melt components are mixed.

of ~1. Most plagioclase derived melts will, therefore, have higher Sr contents and lower Rb/Sr ratios than predicted in a disequilibrium-batch melting model and lie close to the granite Rb–Sr isochron. Under the extreme dissolution rates considered for Fig. 5b equilibrium Rb and Sr K_d's would not apply for biotite (e.g., Sr data of Giletti (1991b) and, given that Rb, as a major structural component of biotite, would probably have a lower D than Sr). Hence, under the parameters of this model, after initial melt formation, Rb and Sr diffusion will be too slow to maintain chemical equilibrium in biotite and $K_{d\ EF}$ will be ~1. Melts would, therefore, have higher Rb/Sr than predicted by a disequilibrium-batch melting model and lie close to the granite Rb–Sr isochron. Two hypothetical melt evolution paths are shown in Fig. 5b with variable proportions of biotite and plagioclase entering the melt. Predicting the trace element and isotopic compositions of actual melts, even in this simple system, requires a knowledge of the melting rates of the minerals.

Thermal modelling implies that melting at Mono Lake occurred in 1.5 years and that the liquid remained in contact with the residue for up to 12 years. During this time the degree of melting in the rocks studied varied from 10 to 70%. Given an original grain size in the protolith of ~0.5 cm, this implies that the minimum linear mineral dissolution rate was 0.7 to 4.6×10^{-10} cm/s. Therefore, the effective diffusional length of an element must exceed this value in order to preserve chemical equilibration between the melt and residual phase. Published diffusion coefficients of many elements are $< 10^{-14}$ cm^2/s in many major and minor rock-forming minerals even at 1000°C (e.g., Brady, 1995). At melting rates of $\sim 10^{-10}$ cm/s diffusion rates of most trace elements would be insufficient to maintain chemical equilibrium unless the effective diffusion distance is on the order of a few microns. Mono Lake is, therefore, an excellent environment in which to test which of the two melting models discussed above is most realistic.

The mineralogy of the Mono Lake granite is relatively simple and biotite would become quickly exhausted during melting. Most of the melting is dominated by quartz–feldspar eutectic melting. The Sr contents of the LOW glasses at Mono Lake are comparable to that of biotite (~30 ppm). The low $^{87}Sr/^{86}Sr$ of these melts, however, implies that most of the Sr was derived from feldspars which in turn implies that $K_{d\ EF}$ cannot have been 1. Interpreting the situation is slightly complicated by the crystallisation of feldspar microlites during cooling of the melt which will have raised the Rb/Sr ratio of the hand-picked glasses. It is clear, however, that there has been significant fractionation in Rb/Sr ratios during the melting event. Further support for small scale equilibrium comes from the observation that anorthoclase and host glass from sub-samples of the extensively melted granite block define Rb–Sr isochrons that are within error of the ^{40}Ar–^{39}Ar age (11.9 ± 0.2 Ma for both 6700-A and 6700-B, Table 2). This demonstrates that Sr isotope equilibrium was attained on a very local scale. The anorthoclase grains are characterised by a spongy texture with a large surface area. The Sr content of anorthoclase is >700 ppm and ~100 ppm in the host glass; i.e., Sr K_d of ~7. Using the formulations of Blundy and Wood (1991) we calculate that the equilibrium K_d for Sr should be ~9. Given the uncertainty in the calculation (e.g., the influence of small compositional variations) this calculation suggests that partitioning of Sr was close to an equilibrium process. Although minor phases such as apatite will influence Sr partitioning between the protolith and the melt, it is clear that the major rock-forming minerals (i.e., feldspar) have retained Sr and that partition coefficients were close to equilibrium values; $K_{d\ Effective} - K_{d\ Equilibrium} \neq 1$. Therefore, even with the evidence of isotopic disequilibrium and the extremely rapid melting rates at Mono Lake, any disequilibrium melting model must have near equilibrium partition coefficients (e.g., Fig. 5a). Despite the melt remaining in the source, the extreme melt heterogeneity implies that, on the scale of sampling (1 cm^2), a fractional melting model is more applicable than a batch melting model.

The geological setting under consideration is undoubtedly atypical of granitoid genesis, if only for the fact that melt was trapped in the source region. The calculated melting rate was so extreme that the diffusional length of most trace elements during the melting event was close to zero but surprisingly partition coefficients appear to have operated. Before assessing the implications of this conclusion to petrogenetic models applied to igneous and metamor-

phic petrology we will consider other cases of crustal anatexis to see if these conclusions hold.

3.2. Seram

The observation of Sr isotope differences between granites and their assumed source regions (Fig. 3) resulted in authors advocating additional unexposed sources (Peucat et al., 1988) or homogenisation of protoliths by the pervasive movement of metamorphic or basinal derived fluids (Wickham, 1990). These conclusions are not favoured for the granites from Seram due to the simple tectonic setting (i.e., a restricted melting region) and the lack of significant fluid movement (i.e., the absence of syn-metamorphic quartz/calcite veins or zones of increased hydration). The simplest explanation for the observed Sr isotope differences between the granites and their source rocks (Fig. 3b) is that minerals in the metasediments did not attain isotopic equilibrium during the thermal event. Rb/Sr ratios of the granites are higher than the protolith whereas the $^{87}Sr/^{86}Sr_{6\,Ma}$ ratios are lower. This observation is consistent with melts forming by disequilibrium melting with a relatively large proportion of feldspar entering the melt (Fig. 5a). The large inter-mineral Sr isotope disequilibrium retained by the migmatites and metasediments (Fig. 4) demonstrate that the granites and their source rocks did not attain isotopic equilibrium during anatexis, even at the scale of the sampled rock chips (~ 7 cm^2).

Despite the evidence for disequilibrium melting in the Sr isotope system, the Nd isotope ratios of the sediments and granites are similar (Fig. 3). In addition the minor differences between the Pb isotope ratios of these rock types are only just outside analytical uncertainty (Fig. 3a). This implies that either the duration of the thermal event was sufficiently long to cause inter- and intra-mineral isotopic equilibrium for Nd and Pb, possibly due to the small grain size of minerals, or that there was no isotopic disequilibrium in the source because all minerals had similar parent–daughter ratios (e.g., Sm/Nd). Further studies are required on coarser-grained rocks to assess the possible extent of Nd and Pb isotope disequilibrium during anatexis.

Published Sr diffusion coefficients imply that the rate of Sr isotope equilibration of minerals within the metasedimentary protolith follows the order biotite > muscovite > oligoclase (Brady, 1995). This means that during the thermal event at ~ 6 Ma, micas and plagioclase in metasediments may have undergone very different degrees of Sr isotope equilibration. Although the effective grain size of the minerals has to be established, the metasediments can be envisaged as consisting of two sub-systems formed by mineral portions that did (i.e., mainly micas) and did not (i.e., mainly plagioclase) reach Sr isotope equilibration. Plagioclase grains in particular could develop a Sr isotope zonation representing equilibrated (e.g., rims and newly grown phases) and unequilibrated (e.g., cores) portions. The $^{87}Sr/^{86}Sr$ of any newly formed metamorphic phase would depend on the equilibration history of the minerals that reacted to produce it. Consequently, we envisage that the $^{87}Sr/^{86}Sr$ of granites at Seram were determined by the relative mass fraction of each mineral portion entering the melt (i.e., equilibrated vs. unequilibrated) and the effective element partition coefficients ($K_{d\,EF}$). The ''future ages'' obtained from the melanosomes, e.g., plagioclase–matrix pairs of BK 21B (Fig. 4), imply that the matrix contains, in addition to micas, a significant amount of unequilibrated plagioclase. The ''ages'' > 6 Ma from the leucosome BK 21A (e.g., muscovite–plagioclase pairs, Fig. 4) and feldspar–whole rock pairs of the granite BK 18 (Table 2), are consistent with feldspar being mainly composed of an unequilibrated restitic component that is incorporated into the granitic melts.

Due to the nature of the obduction process that caused metamorphism of the protolith, minerals were heated relatively rapidly from ambient temperatures of < 300 to $\sim$ 740°C. The amount of time to reach 740°C and the duration of the melting event is only constrained to an order of magnitude but clearly was insufficient to allow Sr isotope equilibration in the protolith. Using published diffusion coefficients for oligoclase at 740°C it can be shown that < 50% of the Sr in 0.5 mm diameter oligoclase grains would exchange with the matrix in 100 ka (calculations following Crank (1975)). The outer 100-μm rim of the grain would be close to full Sr isotope equilibration. The observed Sr isotope disequilibrium implies that, despite the extensive mineral reactions and recrystallisation associated with the metamorphic event, feldspars behaved such that the effective equi-

libration distance of Sr isotopes was significantly below the observed grain size of the protolith (< 0.5 mm).

The granites produced at Seram have migrated from their source and may have undergone fractional crystallisation. In addition, they contain xenocrystic phases so that it is difficult to interpret the granite compositions in terms of melting alone. The Rb/Sr ratios of the granites are higher than the protolith whereas the $^{87}Sr/^{86}Sr_{6\,Ma}$ ratios are lower which demonstrates that melts are not simply derived from mica breakdown reactions. Estimating the exact mineralogy that contributed to melt generation is difficult because the protolith has undergone retrograde metamorphic reactions. Hence, at the time of anatexis the mineralogy and mineral isotopic ratios are poorly constrained. Unfortunately, due to these complications it is impossible to use mass balance calculations to determine the Rb/Sr and $^{87}Sr/^{86}Sr$ of melts in order to determine if equilibrium K_d were in operation. The increased Rb/Sr ratios in the granites does, however, establish that the bulk were $\neq 1$.

The data presented in this study, therefore, suggest that, as with melting at Mono Lake, the short duration of the thermal pulse and the fast melting rate prevented Sr isotope equilibrium, although element partitioning was close to an equilibrium process $K_{d\,EF}$–$K_{d\,EQ}$. Given the rapid melt formation at Mono Lake and Seram it appears unlikely that $K_{d\,EF}$ would ever equal 1 in any geological environment. We can only speculate that under anatectic conditions defects in mineral structures have a fundamental controlling influence on trace element diffusion and that over distances of a few microns Sr diffusion is almost instantaneous, due to mineral reactions and annealing of structural defects. If correct this would imply that $K_{d\,EQ}$–$K_{d\,EF}$ under almost all melting conditions. In contrast, over distances of > 100 μm diffusion behaves in a manner similar to that predicted by simple diffusion equations (e.g., Crank, 1975) such that full Sr isotope equilibrium is not maintained between melts and residue. As with the Mono Lake example, it could be argued that the tectonic environment was atypical of that involved in granitoid genesis. However, P–T conditions are similar to mid-crustal values and hence the data are relevant to any discussion of the processes that lead to granite genesis. Regional migmatite terranes also provide important information and are discussed below.

4. Evidence from regional migmatite terranes and granite bodies

Migmatite complexes represent regions of the crust that have undergone high grade metamorphism for extended periods of time (> 1 Ma) with inferred heating rates in the order of 10°C/Ma (e.g., Vance and O'Nions, 1992). Consequently, they are liable to have undergone greater degrees of chemical and isotopic equilibration than the above examples and are considered by some to represent realistic granite source regions (see Brown, 1994 for review). The interpretation of chemical relations in migmatite complexes is, however, a matter of debate (see Brown et al., 1995 for recent review). This is due to the difficulty in establishing unambiguous source–melt relationships and the degree to which the system has remained closed (i.e., have water or melts left or entered the protolith?). In fact some workers question if leucosomes in migmatites actually represent frozen melts and some have suggested a cumulate origin (Ellis and Obata, 1992). Migmatites frequently record multiple generations of leucosomes (pre-, syn- and post-deformation) and the protolith is known to have undergone significant mineralogical changes due to changing P–T conditions and melting. Hence, determining source–melt relationships and the mineralogy at the time of anatexis is extremely difficult. In this work, we will accept reported field relations at face value in order to assess if any constraints can be placed on the likely rate of melt segregation and extraction and the degree of isotopic equilibration within the protoliths.

A geochemical study of the leucosomes generated from anatexis of mafic rocks in the Grenville Front, Quebec established that some contain Zr and P contents that are between 10 and 50% of that calculated to be in chemical equilibrium with the minerals in the protolith. Consequently, based upon the calculated rate of diffusion of Zr and P in granitic melts, Sawyer (1991) estimated that melts must have been segregated from their source within ~ 20 years, otherwise, the melts would have reached saturation in these elements. Following the same line of reason-

ing, Ayres et al. (1996) estimated that Himalayan tourmaline leucogranites remained in contact with their source for less than 50 ka and maybe less than 7 ka. Similarly, Watt et al. (1996) concluded that leucosomes of the Caledonian Kirtomy Nape, NE Scotland, were formed within 10 ka. Such calculations make the assumption that all minor phases are in contact with the melt, something that does not appear true due to the armouring capability of phases such as garnet and biotite. The above workers argue that their estimates of the rate of melt segregation are reasonable given that Watson et al. (1989) concluded, based upon thermodynamic considerations, that accessory phases would generally occur at grain boundaries. Irrespective of this discussion, melt formation in the regional migmatite discussed above is shown to be a non-batch melting process because the melt is not in chemical equilibrium with the entire residual mineralogy. Further evidence that formation of extensive Himalayan leucogranite complexes may be a disequilibrium process comes from the fact that individual massifs are isotopically heterogeneous (e.g., Manaslu Granite, Deniel et al., 1987) and that the $^{87}Sr/^{86}Sr$ of leucogranites and metasedimentary protoliths are different (Harris and Ayres, 1998). All these data provide compelling evidence for rapid melt segregation and extraction from their protolith and provide further support for arguments in favour of deformation-driven segregation and extraction mechanisms (Clemens and Mawer, 1992; Sawyer, 1994; Petford, 1995; Rushmer, 1995; Rutter and Neumann, 1995). Numerous other studies of migmatite terranes have concluded that they formed by disequilibrium partial melting (e.g., Mehnert and Büsch, 1982; Weber and Barbey, 1986; Wickham, 1987b; Barbey et al., 1989; Burton and O'Nions, 1990; Watt and Harley, 1993; Barbero et al., 1995). Some modern studies, however, conclude that migmatites can form under conditions of chemical equilibrium (e.g., Sawyer, 1987; Barbey et al., 1990; see also review by Brown (1994)).

It is possible to argue that most migmatite terranes were formed at relatively low pressure, mid-crustal levels (Bohlen and Mezger, 1989), whereas granites are formed in deeper, hotter parts of the crust which would have undergone greater isotopic equilibration (see more discussions in (Brown, 1994)). However, it is perhaps important to note that there are very few detailed combined textural–chemical–isotopic studies that establish if granites represent homogeneous melts extracted from a source that was in chemical and isotopic equilibrium. The zoned petrographic nature of many plutons and the large range of trace element contents implies that granitic melts are far from homogeneous bodies. The large range in Rb/Sr ratios have been used to determine WR isochrons but some of these ''ages'' have now been shown to be incorrect with modern U–Pb chronology (e.g., De Later et al., 1981) again possibly suggesting that the source protolith did not reach isotopic equilibrium.

In conclusion, it must be stated that available evidence from migmatite terranes and granitic bodies, although not definitive, does imply that chemical and isotopic disequilibrium occurs during granite genesis. Considering that these terranes have generally undergone high grade metamorphism for extended periods of time (>1 Ma), the evidence of isotopic and chemical disequilibrium during anatexis in these regions reinforces the conclusion made in previous sections that diffusion is sufficiently slow on length scales >100 μm that chemical and isotopic disequilibrium are not maintained. Disequilibrium implies that melting and segregation must be a relatively rapid process, which in turn suggests that in migmatite terranes melting must be episodic. This further implies that melting is probably controlled by the supply of heat and/or water which induces specific melt reactions (e.g., Ayres et al., 1996).

5. Implications

Even if we accept that the evidence of isotopic disequilibrium in some anatectic terranes is atypical of granitic source regions, the data discussed above may still have important implications for many igneous and metamorphic processes.

5.1. Dating metamorphic events

Perhaps the most important implications of the isotopic disequilibrium preserved during anatexis are for radiometric dating of metamorphic rocks. Most

Table 6
Batch equilibrium melting of metasediment under isotopic disequilibrium

1-Ga metasedimentary protolith[a]								
	WR	qz	bt	als	musc	pl	gt	gt new
Mode		0.3	0.3	0.02	0.1	0.23	0.05	0
	Reactant phases					Products		
(1) musc + pl + qtz = liq + als (H_2O from bl)	musc	pl	qz		to	liq	als	
	0.48	0.24	0.28			0.83099	0.16901	
(2) bt + pl + qz + als = liq + gt	bt	pl	qz	als	to	liq	gt new	
	0.41	0.22	0.31	0.06		0.70204	0.29796	
(3) gt + als = liq + spi + qz (% assumed from Table 5 of Patiño Douce and Johnston (1991))	als	gt cor	gl rim	pl	to	liq	qz	sp
	0.11	0.04	0.7	0.15		0.5	0.25	0.25
	Chemical composition and K_d							
	WR	qz	bt	als	musc	pl	gt	gt new
[Rb] ppm	235.5	0	720.3		170.4	10.4	0	0
[Sr] ppm	121.5	0	5		50	500	0	0
$^{87}Sr/^{86}Sr_{1Ga}$	0.708		0.708		0.708	0.708		
Rb/Sr	1.939	0	144.1		3.409	0.021	0	0
$^{87}Rb/^{86}Sr$	5.653	0	1000		10	0.06	0	0
$^{87}Sr/^{86}Sr$	0.7888		15.01		0.8510	0.7089		0
K_d Sr			0.1		0.5	3		
[Sm] ppm	0.77		0.83		0.91	0.73	5.29	0
[Nd] ppm	3.88		5		5	7.31	4	(1.5)
$^{143}Nd/^{144}Nd_{1Ga}$	0.511		0.511		0.511	0.511	0.511	
Sm/Nd	0.1985		0.1655		0.1820	0.0993	1.3222	0
$^{147}Sm/^{144}Nd$	0.12		0.1		0.11	0.06	0.8	
$^{143}Nd/^{144}Nd$	0.51179		0.51166		0.51172	0.51139	0.51625	0.51166
K_d Nd			0.3		0.3	0.2	0.5	0.5

Degree of melting (F)		$^{87}Sr/^{86}Sr$	$^{143}Nd/^{144}Nd$	$^{147}Sm/^{144}Nd$ assumed	T_{CHUR} (Ga)
0.05		0.77503	0.51153	0.12	2.20
0.17	musc out–biot in	0.75662	0.51150	0.12	2.24
0.5		0.96835	0.51157	0.12	2.11
0.69	biot out–gt in	0.82302	0.51157	0.12	2.11
0.75		0.70886	0.51231	0.12	0.66
WR		0.78885	0.51179	0.12	1.69

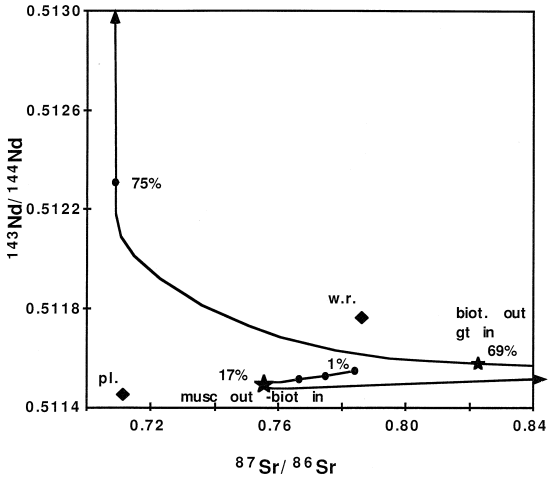

Fig. 6. $^{87}Sr/^{86}Sr$ vs. $^{143}Nd/^{144}Nd$ evolution of batch equilibrium melts from a sediment metamorphosed at 1.0 Ga. Full details of the model are given in Table 6. Melting curve is marked with the degree of melting. Note the extreme variability of both Sr and Nd isotope compositions as melting proceeds. Nd model ages of the protolith is 1.7 Ga whereas model ages of the melts vary from 2.24 to 0.66 Ga. For simplicity this model assumes no REE-bearing minor phases in the protolith and that there is no inter-mineral equilibration which results in more extreme isotopic ratios than expected in nature. wr = whole rock; musc = muscovite; pl = plagioclase; biot = biotite; gt = garnet.

rock dating techniques make the fundamental assumption of isotopic equilibrium between all phases in the rock. The apparent widespread preservation of isotopic disequilibrium indicates that mineral–whole rock or mineral–mineral pairs may yield erroneous ages, as observed at Seram. It, therefore, appears that estimates of mineral growth rates using Nd and Pb isotope systematics of garnets and their host rocks could be wrong, particularly if the rocks contain minor phases (Mezger et al., 1989, 1991; Burton and O'Nions, 1991; Vance and O'Nions, 1992). A reliable age determination requires an isochronous relationship involving several phases. We conclude that a better assessment of isotopic (dis)equilibrium in common rock-forming minerals in high-grade metamorphic rocks is required prior to dating the timing of thermal events that are subsequently used in modelling the physical processes in the Earth's crust.

5.2. Quantification of assimilation–fractional crystallisation (AFC) and partial melting

Many studies have inferred that igneous rocks have assimilated crustal material (DePaolo, 1981). Some AFC models have ascribed arbitrary and unconstrained parameters and often fail to explain combined major, trace element and isotopic variations (e.g., Thirwall and Jones, 1983; Roberts and Clemens, 1995). This has led to some relatively ad hoc models that advocate selective element addition (e.g., Dickin, 1981; Blichert-Toft et al., 1992; Michaud, 1995). The Mono Lake example explains why most combined trace element and isotopic AFC models do not yield coherent results. This example demonstrates how melting will produce a sequence of chemically distinct melts that are in marked isotopic disequilibrium with the crustal source.

To illustrate the difficulties of modelling melting and AFC processes fully, a hypothetical pelitic rock has been subjected to melting. Melting relationships follow Patiño Douce and Johnston (1991) and are presented in Table 6. For simplicity we will confine the discussion to the effects on the Sr–Nd isotope systems caused by the major rock-forming minerals alone. Fig. 6 illustrates how disequilibrium batch melting of a pelite would proceed. Note that only by chance would the melt be in isotopic equilibrium with the crustal source. Notably, garnet in the residue causes significant Nd isotope disequilibrium, in addition to any contribution from minor phases. Estimated Nd model ages (T_{CHUR}) for the melts derived in Fig. 6 range from 0.66 to 2.24 Ga, starting from a protolith with a model age of 1.7 Ga. Consequently, as pointed out previously, Nd model ages will yield unrealistic estimates of the crustal residence age of anatectic melts (e.g., Ayres and Harris, 1997). This admittedly simplistic diagram demonstrates that it is impossible to predict the nature of any AFC process unless the melting relationships and the extent of inter-mineral isotopic equilibrium are known. The

Note to Table 6:
[a] Metasedimentary protolith following melting reactions of Patiño Douce and Johnston (1991) at 10 kbar. Assuming no accessory phases, i.e., Sm–Nd systematics controlled by major phases.

Table 7
AFC of metasediment under conditions of isotopic disequilibrium (assimilated protolith as in Table 6)

AFC parameters			
Assimilant	basalt	bulk D for Sr	1.2
[Sr] ppm	500	*r*	0.4
$^{87}Sr/^{86}Sr$	0.704		

Degrees of crystal fractionation (F)	Sr contents and Sr isotope ratios of melt after assimilation of individual minerals and bulk rock							
	Whole rock		Plagioclase		Muscovite		Biotite	
	Sr	$^{87}Sr/^{86}Sr$	Sr	$^{87}Sr/^{86}Sr$	Sr	$^{87}Sr/^{86}Sr$	Sr	$^{87}Sr/^{86}Sr$
1	500	0.704	500	0.704	500	0.704	500	0.704
0.9	458	0.7055002	483	0.7043	453	0.7051	450	0.7146
0.8	416	0.7073	467	0.7047	407	0.7064	401	0.7278
0.7	374	0.7095	450	0.7051	360	0.7081	351	0.7448
0.6	332	0.7123	433	0.7055	313	0.7103	301	0.7673
0.5	291	0.7158	417	0.7059	267	0.7132	252	0.7987
0.4	249	0.7206	400	0.7064	220	0.7174	202	0.8456
0.3	207	0.7273	383	0.7070	173	0.7238	152	0.9231
0.2	165	0.7374	367	0.7075	127	0.7350	103	1.0756
0.1	123	0.7543	350	0.7082	80	0.7591	53	1.5137

AFC of metasediment under conditions of isotopic disequilibrium are given in Table 7.

5.3. Crustal melting

It could be argued that major volumes of anatectic granites are produced deep in the crust at $\sim$800–900°C and that thermal perturbations are sufficiently long to achieve isotopic equilibrium. The extent of isotopic equilibrium is directly proportional to the duration of heating events, but inversely proportional to the square of the radius of mineral grains (Crank, 1975). Determining the effective diffusional length scale in minerals is, therefore, fundamental. This work appears to imply that the effective diffusional domains are >100 μm. Calculations indicate that in medium- to coarse-grained lower crust rocks (1–10 mm), Sr and Nd isotope equilibrium in feldspar and minor phases, respectively could require up to several tens of millions of years. If correct, full Nd and Sr isotope equilibrium will not be maintained during anatexis. Consequently, studies that have used Nd model ages of granites and metasediments to erect crustal growth models (e.g., Jacobsen, 1988) or to determine the relative mass fractions of mantle and crustal components in the granite magmas (Nelson and DePaolo, 1985) may be questionable. Clearly, further work is required to constrain the effective diffusional length scale of trace elements in metamorphic rocks.

Acknowledgements

Thanks to A. Heumann and T. Elliott for commenting on early drafts of the manuscript and D. Vance and M. Thoni for very constructive reviews. W.J. Lustenhouwer assisted with microprobe analysis. Facilities for isotopic and microprobe analyses were provided by the Vrije Universiteit, Amsterdam and NWO, The Netherlands Scientific Research Council. This is NSG publication 990204.

References

Allégre, C.J., Minster, J.F., 1978. Quantitative models of trace element behaviours in magmatic processes. Earth Planet. Sci. Lett. 38, 1–25.

Al-Rawi, Y., Charmichael, I.S.E., 1967. A note on the natural fusion of granite. Am. Mineral. 52, 1806–1814.

Ayres, M., Harris, N., 1997. REE fractionation and Nd-isotope disequilibrium during crustal anatexis: constraints from Himalayan leucogranites. Chem. Geol. 139, 249–269.

Ayres, M., Harris, N., Vance, D., 1996. Possible constraints on

anatectic melt residence times from accessory mineral dissolution rates: an example from Himalayan leucogranites. Mineral. Mag. 61, 29–36.

Baker, D.R., 1996. Granite melt viscosities: empirical and configurational entropy models for their calculation. Am. Mineral. 81, 126–134.

Barbero, L., Villaseca, C., Rogers, G., Brown, P., 1995. Geochemical and isotopic disequilibrium in crustal melting: an insight from anatectic granitoids from Toledo, Spain. J. Geophys. Res. 100, 15745–15765.

Barbey, P., Bertrand, J.-M., Angoua, S., Dautel, D., 1989. Petrology and U/Pb geochronology of the Telohat migmatites, Aleksod, Central Hoggar, Algeria. Contrib. Mineral. Petrol. 101, 207–219.

Barbey, P., Macauderie, J., Nzenti, J.P., 1990. High-pressure dehydration melting of metapelites: evidence from migmatites of Yaoundé (Cameroon). J. Petrol. 31, 401–427.

Bea, F., 1996. Controls on the trace element composition of crystal melts. Trans. R. Soc. Edinburgh 87, 33–41.

Bédard, J.H., 1989. Disequilibrium mantle melting. Earth Planet. Sci. Lett. 91, 359–366.

Blichert-Toft, J., Lesher, C.E., Rosing, M.T., 1992. Selectively contaminated magmas of the Tertiary East Greenland macrodike complex. Contrib. Mineral. Petrol. 110, 154–172.

Blundy, J.D., Wood, B.J., 1991. Crystal–chemical controls on the partitioning of Sr and Ba between plagioclase feldspar, silicate melts and hydrothermal solutions. Geochim. Cosmochim. Acta 55, 193–209.

Bohlen, S.R., Mezger, K., 1989. Origin of granulite terranes and the formation of the lowermost continental crust. Science 244, 326–329.

Bohlen, S.R., Eckert, J.O., Hankins, W.B., 1995. Experimentally determined solidi in the Ca-bearing granite system $NaAlSi_3O_8$–$CaAl_2SiO_8$–$KAlSi_3O_8$–SiO_2–H_2O–CO_2. Am. Mineral. 80, 752–756.

Brady, J.B., 1995. Diffusion data for silicate minerals, glasses and liquids. In: Ahrens, T.J. (Ed.), Mineral Physics and Crystallography. A Handbook of Physical Constants. AGU, Washington DC, pp. 269–290.

Brown, M., 1994. The generation, segregation, ascent and emplacement of granite magma: the migmatite-to-crustally derived granite connection in thickened orogens. Earth Sci. Rev. 36, 83–130.

Brown, M., Rushmer, T., Sawyer, E.W., 1995. Introduction to special section: mechanisms and consequences of melt segregation from crustal protoliths. J. Geophys. Res. 100, 15551–15563.

Burton, K.W., O'Nions, R.K., 1990. The time scale and mechanism of granulite formation of Kurunegala, Sri Lanka. Contrib. Mineral. Petrol. 106, 66–89.

Burton, K.W., O'Nions, R.K., 1991. High resolution garnet chronometry and the rates of metamorphic processes. Earth Planet. Sci. Lett. 107, 649–671.

Clemens, J.D., Mawer, C.K., 1992. Granite magma transport by fracture propagation. Tectonophysics 204, 339–360.

Cherniak, D.J., 1996. Strontium diffusion in sanidine and albite and general comments on strontium diffusion in alkali feldspar. Geochim. Cosmochim. Acta 60, 5037–5043.

Cherniak, D.J., Watson, E.B., 1992. A study of strontium diffusion in K–feldspar, Na–K feldspar and anorthite using Rutherford backscattering spectroscopy. Earth Planet. Sci. Lett. 113, 411–425.

Cherniak, D.J., Watson, E.B., 1994. A study of strontium diffusion in plagioclase using Rutherford backscattering spectroscopy. Geochim. Cosmochim. Acta 58, 5179–5190.

Chesterman, C.W., 1968. Volcanic Geology of the Bodie Hills, Mono County, CA. GSA Mem. 116.

Crank, J., 1975. The Mathematics of Diffusion. Oxford Univ. Press, 414 pp.

De Later, J.R., Libby, W.G., Trendall, A.F., 1981. The older Precambrian geochronology of Western Australia. Geol. Soc. Aust., Spec. Publ. 7, 145–157.

Deniel, C., Vidal, P., Fernandez, A., Le Fort, P., Peucat, J.-J., 1987. Isotopic study of the Manaslu granite (Himalaya, Nepal): inferences on the age and source of Himalayan leucogranites. Contrib. Mineral. Petrol. 96, 78–92.

DePaolo, D.J., 1981. Trace element and isotopic effects of combined wall-rock assimilation and fractional crystallisation. Earth Planet. Sci. Lett. 53, 189–202.

Dickin, A.P., 1981. Isotope geochemistry of Tertiary igneous rocks from the Isle of Skye, NW Scotland. J. Petrol. 22, 155–189.

Ellis, D.J., Obata, M., 1992. Migmatite and melt segregation at Cooma, New South Wales. Trans. R. Soc. Edinburgh: Earth Sci. 83, 95–106.

Emerman, S.H., Marret, R., 1990. Why dikes?. Geology 18, 231–233.

Fyfe, W.S., 1973. The granulite facies, partial melting and the Archaean crust. Phil. Trans. R. Soc. Lond. A 273, 457–461.

Gast, P.W., 1968. Trace element fractionation and the origin of tholeiitic and alkaline magma types. Geochim. Cosmochim. Acta 32, 1057–1086.

Giletti, B.J., 1991a. Rb and Sr diffusion in feldspars, with implications for cooling histories of rocks. Geochim. Cosmochim. Acta 55, 1331–1343.

Giletti, B.J., 1991b. Diffusion kinetics of Mg, Ca, Sr and Ba in albite and Sr in muscovite and biotite. EOS 72, 529.

Giletti, B.J., Casserly, J.E.D., 1994. Strontium diffusion kinetics in plagioclase feldspars. Geochim. Cosmochim. Acta 58, 3785–3793.

Hanson, G.N., 1977. Geochemical evolution of the suboceanic mantle. J. Geol. Soc. London 134, 235–253.

Harris, N., Ayres, M., 1998. The implications of Sr-isotope disequilibrium for rates of prograde metamorphism and melt extraction in anatectic terrains. In: Treloar, P.J., O'Brien, P.J. (Eds.), What Drives Metamorphism and Metamorphic Reactions? Geol. Soc. London, Spec. Publ. 138, 171–182.

Hart, S.R., Allégre, C.J., 1980. Trace element constraints on magma genesis. In: Hargraves, R.B. (Ed.), Physics of Magmatic Processes. Princeton Univ. Press, Princeton, pp. 121–158.

Henderson, P., Williams, C.T., 1979. Variations in trace element partition (crystal magma) as a function of crystal growth rate. In: Ahrens, L.H. (Ed.), Origin and Distribution of the Elements. Pergamon, Oxford, pp. 191–198.

Hogan, J.P., Sinha, A.K., 1991. The effect of accessory minerals

on the redistribution of lead isotopes during crustal anatexis: a model. Geochim. Cosmochim. Acta 55, 335–348.

Jacobsen, S.B., 1988. Isotopic constraints on crustal growth and recycling. Earth Planet. Sci. Lett. 90, 315–329.

Kaczor, S.M., Hanson, G.N., Eterman, Z.E., 1988. Disequilibrium melting of granite at the contact with a basic plug: a geochemical and petrographic study. J. Geol. 96, 61–78.

Linthout, K., Helmers, H., 1994. Pliocene obducted, rotated and migrated ultramafic rocks and obduction-induced anatectic granite, SW Seram and Ambon, Eastern Indonesia. J. Southeast Asian Earth Sci. 9, 95–109.

Linthout, K., Helmers, H., Wijbrans, J.R., Diederik, J., Van Wees, A.M., 1996. $^{40}Ar/^{39}Ar$ constraints on obduction of the Seram ultramafic complex: consequences for the evolution of the southern Banda Sea. In: Hall, R., Blundell, D. (Eds.), Tectonic Evolution of Southeast Asia. Geol. Soc., Spec. Publ. 106, 455–464.

McKenzie, D.P., 1985. The extraction of magma from the crust and mantle. Earth Planet. Sci. Lett. 74, 81–91.

Mehnert, K.R., Büsch, W., 1982. The initial stages of migmatite formation. Neues Jahrb. Miner., Abh. 145, 211–238.

Mezger, K., Hanson, G.N., Bohlen, S.R., 1989. U–Pb systematics of garnet: dating the growth of garnet in the late Archaean Pikwitonei granulite domain at Cauchon and Natawahunan Lakes, Manitoba, CA. Contrib. Mineral. Petrol. 101, 136–148.

Mezger, K., Rawnsley, C.M., Bohlen, S.R., Hanson, G.N., 1991. U–Pb garnet, sphene, monazite and rutile ages: implications for the duration of high-grade metamorphism and cooling histories, Adirondack Mts. N. Y. J. Geol. 99, 415–428.

Michaud, V., 1995. Crustal xenoliths in recent hawaiites from Mount Etna, Italy. Evidence for alkali exchange during magma–wallrock interaction. Chem. Geol. 122, 21–42.

Miller, C.F., Watson, E.B., Harrison, T.M., 1988. Perspectives on the source, segregation and transport of granitoid magmas. Trans. R. Soc. Edinburgh: Earth Sci. 79, 135–156.

Nelson, B.K., DePaolo, D.J., 1985. Rapid production of continental crust 1.7 to 1.9 by ago: Nd isotopic evidence from the basement of the North American mid-continent. Geol. Soc. Am. Bull. 96, 746–754.

Patiño Douce, A.E., Johnston, A.D., 1991. Phase equilibria and melt productivity in the pelitic system: implications for the origin of peraluminous granitoids and aluminous granulites. Contrib. Mineral. Petrol. 107, 202–218.

Petford, N., 1995. Segregation of tonalitic–trondhjemitic melts in the continental crust: the mantle connection. J. Geophys. Res. 100, 15735–15743.

Petford, N., Kerr, R.C., Lister, J.R., 1993. Dyke transport of granitoid magmas. Geology 21, 845–848.

Peucat, J.J., Jegouzo, P., Vidal, P., Bernard-Griffiths, J., 1988. Continental crust formation seen through the Sr and Nd isotope systematics of S-type granites in the Hercynian belt of western France. Earth Planet. Sci. Lett. 88, 60.

Prinzhofer, A., Allégre, C.J., 1985. Residual peridotites and the mechanisms of partial melting. Earth Planet. Sci. Lett. 74, 251–265.

Rapp, R.P., Watson, E.B., 1986. Monazite stability and dissolution kinetics: implications for the thorium and light rare earth chemistry of felsic magmas. Contrib. Mineral. Petrol. 94, 304–316.

Roberts, M.P., Clemens, J.D., 1995. Feasibility of AFC models for the petrogenesis of calc–alkaline magma series. Contrib. Mineral. Petrol. 121, 139–147.

Rudnick, R.L., 1992. Xenoliths — samples of the lower continental crust. In: Fountain, D.M., Arculus, R., Kay, R.W. (Eds.), Continental Lower Crust. Elsevier, Amsterdam, pp. 269–316.

Rushmer, T., 1995. An experimental deformation study of partially molten amphibolite: application to low-melt fraction segregation. J. Geophys. Res. 100, 15681–15695.

Rutter, E., Neumann, D., 1995. Experimental deformation of partially molten Westerly granite under fluid-absent conditions with implications for the extraction of granitic magmas. J. Geophys. Res. 100, 15697–15715.

Sawyer, E.W., 1987. The role of partial melting and fractional crystallisation in determining discordant migmatite leucosome compositions. J. Petrol. 28, 445–473.

Sawyer, E.W., 1991. Disequilibrium melting and the rate of melt–residuum separation during migmatisation of mafic rocks from the Grenville Front, Quebec. J. Petrol. 32, 701–738.

Sawyer, E.W., 1994. Melt segregation in the continental crust. Geology 22, 1019–1022.

Thirwall, M.F., Jones, A.P., 1983. Isotope geochemistry and contamination mechanisms of tertiary lavas from Skye, northwest Scotland. In: Hawkesworth, C.J., Norry, M.J. (Eds.), Continental Basalts and Mantle Xenoliths. Shiva, pp. 186–208.

Tommasini, S., Davies, G.R., 1997. Isotope disequilibrium during anatexis: a case study of contact melting, Sierra Nevada, CA. Earth Planet. Sci. Lett. 148, 273–285.

Vance, D., O'Nions, R.K., 1992. Prograde and retrograde thermal histories from the central Swiss Alps. Earth Planet. Sci. Lett. 113, 397–409.

Watson, E.B., 1996. Surface enrichment and trace element uptake during crystal growth. Geochim. Cosmochim. Acta 60, 5013–5020.

Watson, E.B., Vicenzi, E.P., Rapp, R.P., 1989. Inclusion/host relations involving accessory minerals in high-grade metamorphic and anatectic rocks. Contrib. Mineral. Petrol. 101, 220–231.

Watt, G.R., Harley, S.L., 1993. Accessory phase control on the geochemistry of crustal melts and restites produced during water-undersaturated partial melting. Contrib. Mineral. Petrol. 114, 550–566.

Watt, G.R., Burns, I.M., Graham, G.A., 1996. Chemical characteristics of migmatites: accessory phase distribution and evidence for fast melt segregation rates. Contrib. Mineral. Petrol. 125, 100–111.

Weber, C., Barbey, P., 1986. The role of water, mixing processes and metamorphic fabric in the genesis of the Baume migmatites. Contrib. Mineral. Petrol. 92, 481–491.

Wickham, S.M., 1987a. The segregation and emplacement of granitic melts. J. Geol. Soc. London 144, 281–297.

Wickham, S.M., 1987b. Crustal anatexis and granite petrogenesis during low-pressure regional metamorphism: the Trois Seigneurs Massif, Pyrenees France. J. Petrol. 28, 127–169.

Wickham, S.M., 1990. In: Ashworth, Brown (Ed.), High Temper-

ature Metamorphism and Crustal Anatexis. Unwin-Hyman, London, 1990, pp. 124–148.
Yardley, B.W.B., 1995. An Introduction to Metamorphic Petrology. Longmann, p. 254.
Zhang, L.S., Schärer, U., 1996. Inherited Pb components in magmatic titanite and their consequences fro the interpretation of U–Pb ages. Earth Planet. Sci. Lett. 138, 57–65.
Zhang, Y., Walker, D., Lesher, C.E., 1989. Diffusive crystal dissolution. Contrib. Mineral. Petrol. 102, 492–513.